Implementation of Dual Control Maximum Power Point Tracking-Based DC–DC Converter Fed Solar PV Power Application

Vijaya Vardhan Reddy P, B L Narasimharaju, *Senior Member, IEEE*, and Hiralal Murlidhar Suryawanshi, *Fellow, IEEE*

***Abstract*—This article presents an effective power extraction methodology from photovoltaic (PV) with a front end dc–dc Resonant converter with dual control. Usually, conventional dc–dc boost converter shows lower efficiency and extra components for soft-switching. Furthermore, converter power transfer efficiency for PV integration is limited. Hence, to address these challenges this article investigates an isolated dc–dc resonant converter with proposed control to attain wider voltage regulation with maximized PV power generation. In addition, this converter can achieve zero-voltage switching under wider operating loads. The proposed control method improves the efficiency even under light load condition without effecting digital-signal-processor resolution, along with a simple pertub and observe maximum power point PI control approach. A 2.2-kW prototype is built and operated to interface PV system and to verify the performance over entire load. The peak efficiency of the converter is found to be 98.7% at (1.1-kW) 50% of the full load.**

***Index Terms*—High frequency (HF), maximum power point tracking (MPPT), resonant network, zero-voltage switching (ZVS).**

I. Introduction

ISOLATED dc–dc converters are widely used for power transformation among power electronics applications. They are typically applied to control dc power, connecting dc loads, energy-storage devices, and generating sources, such as photovoltaic (PV) arrays. Among distributed generation systems, renewable energy sources are green electrical power sources. Moreover, PV power generation is enhancing exponentially due to its clean and abundant in nature compared to fossil fuel-based energy. However, the output voltage and power of a solar panel vary depending on solar irradiation and temperature. Hence, for further popularity of PV systems, it is important to reducing the price and enhance the efficiency and reliability of these systems [1].

To transform varying low-level solar voltage source to constant high-level dc voltages and to simultaneously track the maximum power point, interfacing dc–dc converters play a critical role. The nonisolated boost converter can maintain the constant required level of dc voltage of the solar panel. However, this converter suffers from hard switching of power switches over the wide-input voltage and output load range operation [2], [3]. Previous research has proposed numerous dc–dc converter topologies [4], [5], [6]. In general, single-ended converters and double-ended converters are suitable for such applications [7], [8], [9]. The most straightforward single-ended converter is flyback; regardless of the low cost, the efficiency is relatively poor due to its inability to transfer power directly from the source to the load and low magnetics utilization [10]. Alternatively, resonant topologies are a very intriguing solution because they exhibit sinusoidal current or voltage waveforms that reduce both electromagnetic interference and switching losses [11], [12], [13]. Among the third-order resonant converters, the *LCC* converter has the highest regulation capability among the other converters introduced in the literature. This configuration overcomes the drawbacks of a simple series and parallel resonant circuit, and it requires two independent physical capacitors that are both large. Two inductors and one capacitor form *LLC* resonant converter to get similar characteristics without changing the physical component count. An advantage of *LLC* has relatively improved efficiency at light load conditions as well because the device current decreases as the load current decreases [14], [15], [16]. The application of *LLC* converter is seen in many industrial applications. However, there are limitations on the maximum operating frequency against input voltage and/or output load regulation in a wide range. On the other hand, different control techniques such as switching frequency, duty cycle, phase shift, and hybrid control are used to maintain the constant output voltage of a PV fed dc–dc resonant converter over variation with input voltage. In frequency control switching losses increase rapidly [9], [10], [11], due to sharp increase in frequency excursions from full load

Manuscript received 18 February 2022; revised 25 May 2022, 7 August 2022, and 7 September 2022; accepted 27 September 2022. Date of publication 18 October 2022; date of current version 3 April 2023. This work was supported by Department of Science and Technology and the Indian National Academy of Engineering under Abdual Kalam Technology Innovation National Fellowship under Grant INAE/121/AKF/28. *(Corresponding author: Vijaya Vardhan Reddy P.)*

Vijaya Vardhan Reddy P is with the Varroc Engineering LTD, Aurangabad 431136, India (e-mail: vijaya.reddy@varroc.com).

B L Narasimharaju is with the National Institute of Technology Warangal, Hanamkonda 506004, India (e-mail: blnraju@nitw.ac.in).

Hiralal Murlidhar Suryawanshi is with the NIT Hamirpur, Hamirpur 177005, India (e-mail: hmsuryawanshi@eee.vnit.ac.in).

Color versions of one or more figures in this article are available at https://doi.org/10.1109/TIE.2022.3213891.

Digital Object Identifier 10.1109/TIE.2022.3213891

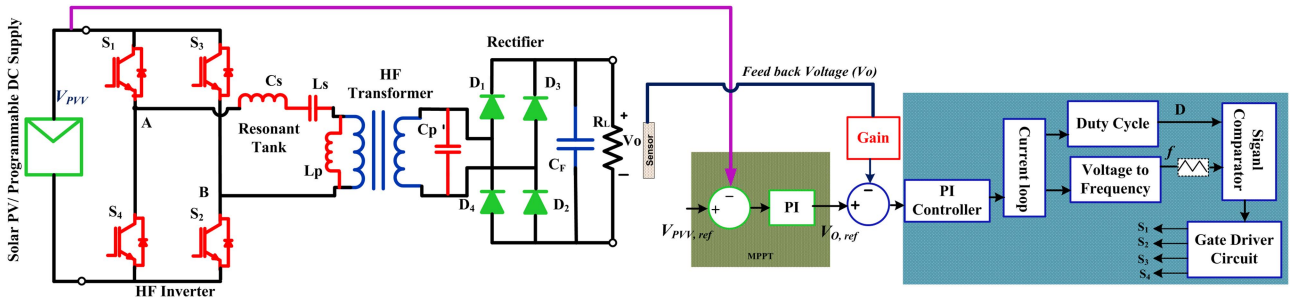

Fig. 1. Block diagram of PV fed MPPT-based dc–dc resonant converter.

to no load. Moreover, it results in nonoptimal magnetic elements as a result of high-frequency (HF) excursions and the effect of electromagnetic interference (EMI) [12], [13]. In case of phase shift and duty cycle, it cannot ensure zero-voltage switching (ZVS) over wider range and transferring power reduced. Furthermore, the hybrid control strategy adapts frequency or duty cycle independently to control the output voltage. However, frequency and duty cycle actions are performed sequentially rather than concurrently, resulting in greater excursion and digital signal processor (DSP) resolution [17], [18]. Additionally, asymmetrical duty cycle may lead core saturation, and voltage regulation at very low-load conditions is challenging; switching frequency excursions increase and deteriorate converter efficiency [19].

Thus, an effective control approach is required to implement maximum power point tracking (MPPT) employing general purpose DSP for effective PV utilization, output voltage regulation of the upstream resonant converter against PV voltage variations and sustained soft switching of the resonant converter over a comprehensive range with narrow frequency operation.

Here, a dual control technique is discussed to overcome the converter performance degradation due to limited action of duty cycle and switching frequency. Initially, duty cycle control is implemented before ZVS fails, later by adjusting both duty cycle and switching frequency sequentially and simultaneously to automatically regulate required output voltage over entire load range, ensure wider ZVS range and narrow frequency operation to achieve better voltage regulation.

The abovementioned resonant converter topologies can operate with varying input voltage to some extent while operating at maximum power point (MPP) but are unable to attain over wide input line voltage regulation, resulting inefficient operation of the overall system. Hence, significant design effort is required for the choice of control method, converter configuration, and integrated power utilities.

Therefore, this article describes the integration of PV-fed dc–dc converter in voltage control mode using dual control method for an MPPT algorithm and effective input line voltage regulation with constrict frequency and duty cycle adaptation. The power circuit consists of a modified *LCLC* series resonant converter with a dual control method where duty cycle and frequency are adjusted to maximize PV power and to maintain the converter output voltage over wider input power variations. The presented experimental results of 2.2 kW converter validate the effectiveness of the proposed approach.

II. Proposed PV Fed Converter System and Operation

Fig. 1 illustrates the proposed dual control MPPT-based converter for renewable energy application. Solar PV voltage V_{PVV} is fed to dc–dc resonant converter, by restricting the variations in frequency and duty cycles, output voltage of the converter is automatically regulated by the PI control. As a result, the variation in switching frequency and duty cycle is limited. Thus, V_{AB} can be expressed as a function of the duty cycle and switching frequency as a Fourier series. The dc component in the expression in the following is zero because of symmetry

$$V_{AB}(t) = \sum_{n=1,3}^{\infty} \frac{2\sqrt{2}V_{\mathrm{PVV}}}{n\pi}\sqrt{1-\cos 2\pi nD}\sin(n\omega_s t + \theta_n) \tag{1}$$

where V_{AB} is HF inverter voltage and θ_n is the phase angle. As a result, the input solar PV source (V_{PVV}) to the converter's output voltage (V_0), the gain (M) for the proposed dual control method is derived as

$$M = \frac{V_0}{V_{\mathrm{PVV}}} = \frac{V_{AB}Z_p}{V_{\mathrm{PVV}}Z_{in}} = \frac{2}{\pi}\frac{Z_p\sqrt{1-\cos 2\pi D}}{Z_{\mathrm{in}}} \tag{2}$$

Z_{in} input impedance and Z_p parallel impedance. The essence of the proposed algorithm is to trap the system within a stable limit while ensuring the required voltage regulation. The dual control method involves simultaneous variation in the two fundamental components of a dc–dc converter, i.e., switching frequency and duty cycle. It is implemented with the help of PI controllers, as shown in Fig. 1, which uses PI controller to control the switching frequency and obtain the duty cycle. The key waveforms of the converter with the proposed control method as shown in Fig. 2. In Fig. 3, design curves compared with the proposed dual control to the conventional method, shows that it has 2-degree control over output voltage. In addition, solar PV is fed directly to the resonant converter without an additional boost converter so that the power density of the system improves. Table I shows the hardware prototype specifications. Furthermore, power generation from solar PV using developed converter with the pertub and observe approach for MPPT discussed in the following section.

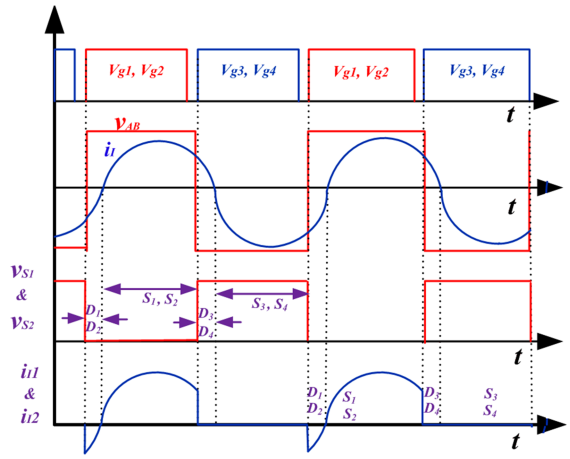

Fig. 2. Key waveforms of the proposed resonant converter.

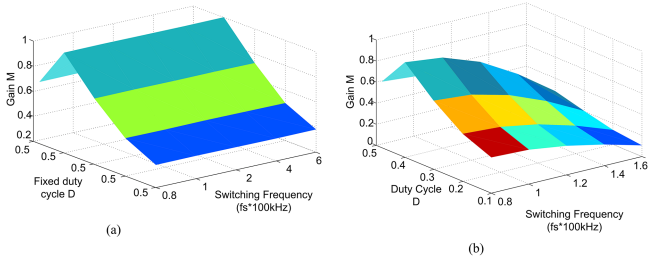

Fig. 3. Optimal design plots. (a) Conventional gain versus switching frequency variation. (b) Proposed gain versus dual control.

TABLE I
SYSTEM PARAMETERS FOR HARDWARE SETUP

Parameter	Values
Input voltage	40 V–60 V
HF transformer	2.2 kW, 100 kHz, n=1:4.6
Series branch parameters	$L_s = 3.35\mu$H; $Cs = 75.9\mu$F
Parallel branch elements	$L_p = 700\mu$H; $C_p = 0.0018\mu$F
Switching frequency (Y_s)	104–150.kHz
Duty cycle	0.25–0.48
Load	22 Ω, 10 A

A. PV Power Generation Using MPPT Algorithm With Proposed Dual Control Method

To maximize the solar PV system's power generation, voltage control mode is considered for programming the MPPT algorithm. Moreover, power balancing between the solar PV system and the prototype dc–dc power converter, MPPT V_{PVV}, is fixed at 48 V to attain maximum power of 2.2 kW conditions. To demonstrate the PV module's MPPT operation, a modified *LCLC*-type resonant converter is used as the power conditioning converter in conjunction with the perturb and observe algorithm in two ways: 1) direct duty perturbation and 2) reference voltage perturbation.

Here, in this article, the PV module voltage reference is used as the control parameter in conjunction with two PI controllers to adjust the duty cycle and the switching frequency of the proposed converter.

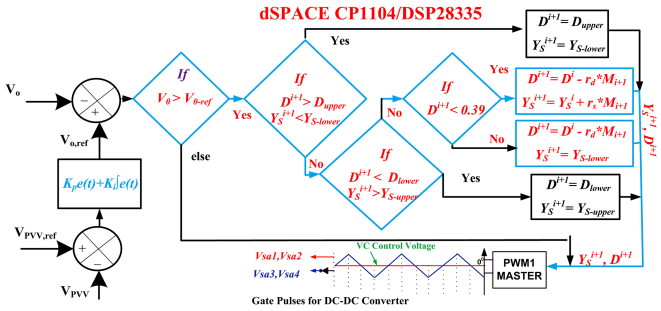

Fig. 4. Flowchart for proposed dual control method to generate gate signals.

From the perspective of a dc–dc resonant converter, maximize the power can be simply referred to as constraining: Mode of voltage control: If irradiation causes MPPT <, i.e., converter output voltage (V_O) tends to decrease, a fine gain adjustment is required to regulate the output voltage. Hence, to adjust the output voltage heeding to irradiation, starting from the full load, the duty cycle is varied. However, controlling the duty cycle will result in ZVS failure in near-light load conditions. In the proposed algorithm, whenever the duty cycle exceeds a certain threshold where ZVS fails, the variable frequency control activates along with the duty cycle. Hence, duty cycle control is adapted prior to ZVS condition failure. Switching frequency and duty cycle are adjusted concurrently based on load variation after ZVS condition failure to regulate the output voltage. Fig. 1 describes a simple MPPT closed algorithm to implement the above logic. Similarly, if irradiation causes MPPT to be >, then V_O increases.

To obtain the maximum reference voltage from the PV panel in the application, the feedback voltage of the panel compared to the maximum PV voltage reference set $V_{\mathrm{PVV,ref}}$. Voltage control mode utilizes PI controller for the closed-loop operation. The MPPT algorithm generates a reference PV voltage with a perturbation frequency of 7.8 Hz and a perturbation size of 1 V. The outer PI regulator takes reference PV voltage and actual PV voltage as the inputs and generates a control signal, i.e., reference output voltage, $V_{O,\mathrm{ref}}$, which is then compared with the actual output voltage, V_O. Finally, the PI controller parameters are regulated to obtain the set reference dc voltage under irradiation and load perturbation to maintain MPPT at ($V_{O,\mathrm{ref}}$) and generate a control signal, v_c. Fig. 4 shows the flowchart of the proposed dual control algorithm to generate the requisite duty cycle and switching frequency parameters. To keep the output voltage constant, the gain of the dc–dc converter must be adjusted with a duty cycle (D) control at a fixed frequency or variable frequency-duty cycle ($Y s$ and D) control depending on the ZVS failure constraint. As a result, the control logic validates the boundary conditions D_{upper}=0.48, $Y_{s\text{-lower}}$=103 kHz and D_{lower}=0.2, $Y_{s\text{-upper}}$=150 kHz. When these constraints are met, duty cycle control is activated to control the required output voltage prior to the failure of ZVS constraint ($D_{\mathrm{crit(zvs)}}$=0.38). When the Dcrit(zvs) condition is met, the frequency-duty cycle is adjusted to maintain a constant output voltage while

TABLE II
COMPARISON OF DIFFERENT CONVERTERS WITH THE PROPOSED CONVERTER

Parameters	E-Asa *et al.* [15]	Navid *et al.* [9]	Chen *et al.* [20]	Hwa *et al.* [16]	S. Ryu *et al.*[21]	Presented Work
Converter type	*CLL* resonant	Resonant *LCLC*	*LCLC* series resonant Converter	LLC resonant converter	Series resonant converter	Modified *LCLC* resonant converter
Power	700 W	1800 W	500 W	240 W	3.3 kW	2.2 kW
No. of switches	Four	Four	Four	Two	Four	Four
No. of diodes	Two	Four	–	Two	Four	Four
Operating Frequency	90–200kHz	100kHz	135–250kHz	1.06 MHz	100–400kHz	104–150.6 kHz
Duty cycle	0.50	0.33–0.45	< 0.50	0.42–0.450	0.30	0.48–0.25
Order of Tank	Third	Fourth	Fourth	Third	Second	Fourth
Resonant Frequency	100kHz	100kHz	100kHz	1.02MHz	100kHz	100kHz
Remarks	L_m used as L_p	L_m used as L_p	Shunt L_p external	L_m used as L_p	–	L_p is used for L_m
Control Operation	Phase Shift and Variable Y_s	Fixed Y_s and Variable duty	Asymmetric Pulse-width	Independent Frequency, Duty cycle	Variable Y_s & Asymmetrical Duty cycle	(Dual Control) Variable Y_s and Duty Cycle
Efficiency (η)	79% to 94% $\eta_{\max}$ 96.2% I_L	89.5% to 95.2% $\eta_{\max}$ 50% I_L	94.1% to 96.20% $\eta_{\max}$ at 60% I_L	84.8% to 92% $\eta_{\max}$ 80% I_L	88.1% to 97% $\eta_{\max}$ 40% I_L	91.8% to 98.7% $\eta_{\max}$ 50% I_L

soft switching. Table II compares the different converters. To implement the abovementioned algorithm, the signal analysis approach is used to determine the relation between output and control as follows.

B. Small-Signal Analysis

The following assumptions were made for the small signal modeling of the converter:

1) all the power semiconductor devices are lossless and ideal;
2) inductor L_s includes the leakage inductance of the HF transformer;
3) snubber/device capacitance charging and discharging intervals are short and neglected.

When the switching state is ON/OFF, the currents and voltages are expressed as

$$Ls\frac{di_{L_s}}{dt} = v_{\text{PVV}} - v_{C_s} - \frac{v_o}{n} \tag{3}$$

$$C_p\frac{dv_o}{dt} = \frac{i_{L_s}}{n} - \frac{v_o}{R_{\text{ac}}} - i_{L_p} \tag{4}$$

$$C_s\frac{dv_{C_s}}{dt} = i_{L_s} \tag{5}$$

$$L_p\frac{di_{L_p}}{dt} = \frac{v_o}{n}. \tag{6}$$

Introducing perturbation around the steady-state values of the state variables i_{L_s} series inductor current, v_o output voltage, v_{C_s} capacitor voltage, i_{L_p} shunt inductor current, and duty cycle (d)

$$i_{L_s} = I_{L_s} + \hat{i}_{L_s}; i_{L_p} = I_{L_p} + \hat{i}_{L_p} \tag{7}$$

$$v_o = V_o + \hat{v}_o; v_{\text{PVV}} = V_{\text{PVV}} + \hat{v}_{\text{PVV}} \tag{8}$$

$$v_{C_s} = V_{C_s} + \hat{v}_{C_s}; d = D + \hat{d}. \tag{9}$$

The currents and voltages are averaging each state by using the duty cycle as a weighting factor. When the switch is OFF, OFF duty cycle $(1-d)$, is multiplied to (3)–(6)

$$Ls\frac{d(i_{L_s}+\hat{i}_{L_s})}{dt} = (V_{\text{PVV}}+\hat{v}_{\text{PVV}}) - (1-D-\hat{d})(V_{C_s}+\hat{v}_{C_s}) - (1-D-\hat{d})\frac{v_o}{n} \tag{10}$$

$$C_p\frac{d(V_o+\hat{v}_o)}{dt} = (1-D-\hat{d})\left(\frac{(i_{L_s}+\hat{i}_{L_s})}{n} - (1-D-\hat{d})(I_{L_p}+\hat{i}_{L_p}) - \frac{V_o+\hat{v}_o}{R_{\text{ac}}}\right. \tag{11}$$

$$C_s\frac{d(V_{C_s}+\hat{v}_{C_s})}{dt} = (1-D-\hat{d})(I_{L_s}+\hat{i}_{L_s}) \tag{12}$$

$$L_p\frac{d(I_{L_p}+\hat{i}_{L_p})}{dt} = (1-D-\hat{d})\frac{(V_o+\hat{v}_o)}{n}. \tag{13}$$

To construct a small-signal ac model at a quiescent operating point, each vector is composed of the equilibrium dc components and ac variations (19), (20) shown at the bottom of next page

$$Ls\frac{d\hat{i}_{L_s}}{dt} = v_{\text{PVV}} - (1-D)V_{C_s}\hat{d} - \frac{V_o}{n}\hat{d} \tag{14}$$

$$C_p\frac{d\hat{v}_o}{dt} = (1-D)\left(\frac{i_{L_s}}{n} - i_{L_p}\right) - I_{L_s}\hat{d} + I_{L_p}\frac{V_o}{R_{\text{ac}}}\hat{d} \tag{15}$$

$$C_s\frac{dv_{C_s}}{dt} = I_{L_s} \tag{16}$$

$$L_p\frac{di_{L_p}}{dt} = \frac{V_o}{n}\hat{d} + \frac{(1-D)}{n}V_o \tag{17}$$

$$\begin{bmatrix}\hat{i}_{L_s}\\ \hat{v}_{C_s}\\ \hat{i}_{C_p}\\ \hat{v}_o\end{bmatrix} = \left[A^{-1}\right]\begin{bmatrix}V_{C_s}+\frac{V_o}{n}\\ -I_{L_s}\\ -\frac{V_o}{n}\\ I_{L_p}-I_{L_s}\end{bmatrix}\hat{d} + [A]^{-1}\begin{bmatrix}1\\0\\0\\0\end{bmatrix}\hat{v}_{\text{PVV}}. \tag{18}$$

The control-to-output transfer function is obtained from (20) by keeping $\hat{v}_{\text{PVV}}$ zero. In comparison to the outer voltage loop,

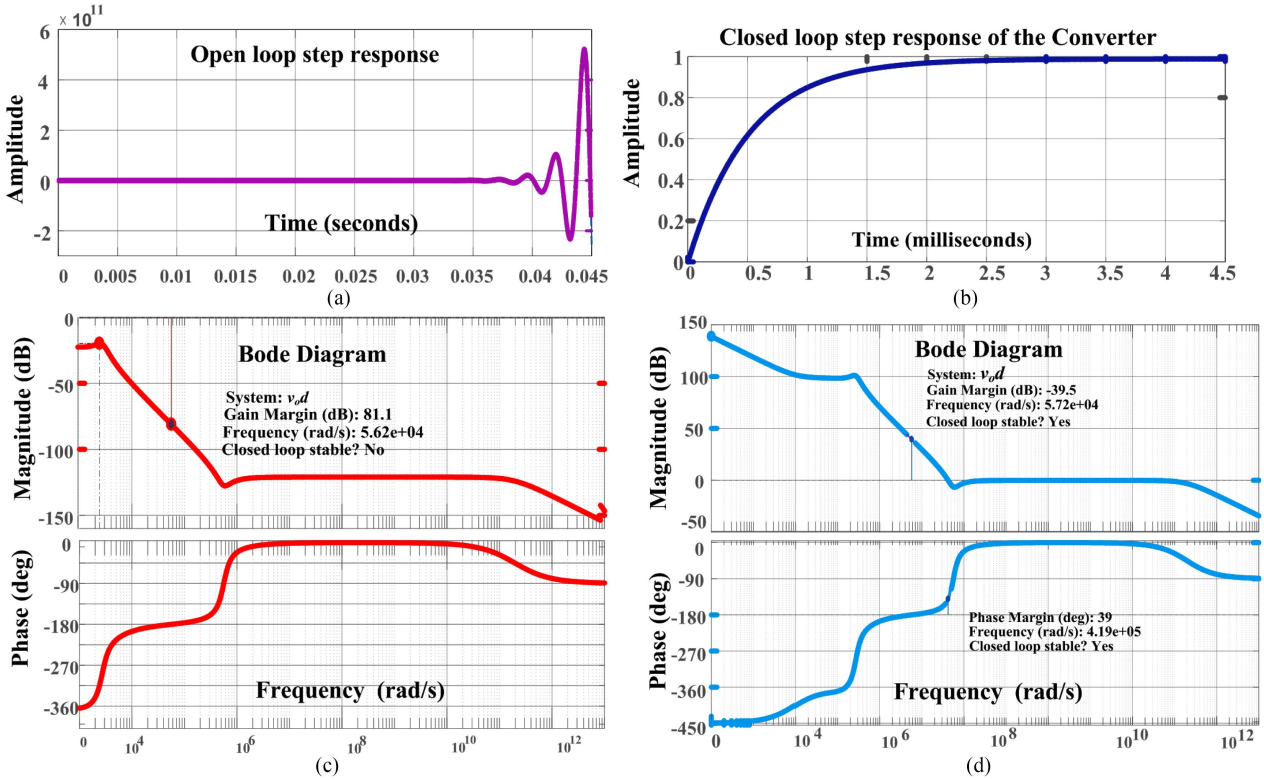

Fig. 5. Response of transfer function output voltage to dutycycle. (a) Open-loop step response. (b) closed-loop step response. (c) Bode plot of uncompensated system in voltage control loop. (d) Bode plot of the compensated voltage control loop system.

the inner current control loop has faster dynamics. As a result, the current-loop dynamics are neglected when designing the voltage controller. Fig. 5(a) shows the open-loop response of the transfer function v_{od} and corresponding frequency response, as shown in Fig. 5(c). Fig. 5(b) shows the closed-loop operation of the system and its stability is shown in Fig. 5(d).

III. Experimental Results

The input source is taken from the Magna (5 kW) programmable dc source with DSP28335 to implement the MPPT algorithm. The effects of different irradiance levels: 1000 W/m^2, 750 W/m^2, 500 W/m^2, and 250 W/m^2, sudden change in irradiance levels, and also temperature change from 25 °C to 40 °C are observed with the proposed control method on the dc–dc converter. In Fig. 6, the PV voltage and PV current tracking are observed with the P and O approach MPPT algorithm. Finally, the experimental setup of solar PV integration with the proposed converter is shown in Fig. 7.

The output voltage is retained at 220 V by raising or reducing the loading on the converter according to the energy obtained from the PV units, as shown in Fig. 6.

In Fig. 6(a), at irradiance level 1000 W/m^2, solar PV input voltage range of 40–60 V to the dc–dc converter with 100% loading 46 A. The proposed P and O approach MPP algorithm tracking effectively tracks the maximum power of 2199 W. Similar to this, Fig. 6(b) shows MPP tracking at 1650 W for 750 W/m^2 of irradiance at the specified input voltage for the converter at 75% loading at 35 A. In Fig. 6(c), solar PV voltage to the dc–dc converter is provided to observe the MPP of 1100 W tracking at an irradiation level of 500 W/m^2. The effect of a loop change in irradiance from 1000 to 750 W/m^2 is captured

$$[A]^{-1} = \frac{\left[sL_p\left(sC_p + \frac{1}{R_{ac}}\right)\right]^2 * s(1-D)}{|A|} \begin{bmatrix} sC_s & (1-D) & 0 & 0 \\ (1-D) & sL_s & 0 & 0 \\ 0 & 0 & sL_sC_s/L_p & 0 \\ -sC_sL_p & L_p(1-D) & -(sL_sC_s+1) & \frac{s^2L_sC_sL_p}{(1-D)} - (1-D)C_p \end{bmatrix} \tag{19}$$

$$\frac{v_o}{d} = \frac{\begin{array}{c} s^3L_sC_sL_p(I_{Ls}-I_{Lp}) + s^2(L_sC_s(1-D)V_o/n + C_sL_p(1-D)(V_{cs}+V_o/n) + s(L_p(1-D)I_{Ls}+ \\ (1-D)^2I_{Ls} - I_{Lp} + (1-D)^3V_o/n \end{array}}{s^4L_sC_sL_pC_o + s^3\frac{C_sL_p}{R_{\text{ac}}} + s^2(L_sC_s(1-D)^2/n + L_pC_o(1-D)^2) + sL_p(1-D)^2/R_{\text{ac}} + (1-D)^4/n}. \tag{20}$$

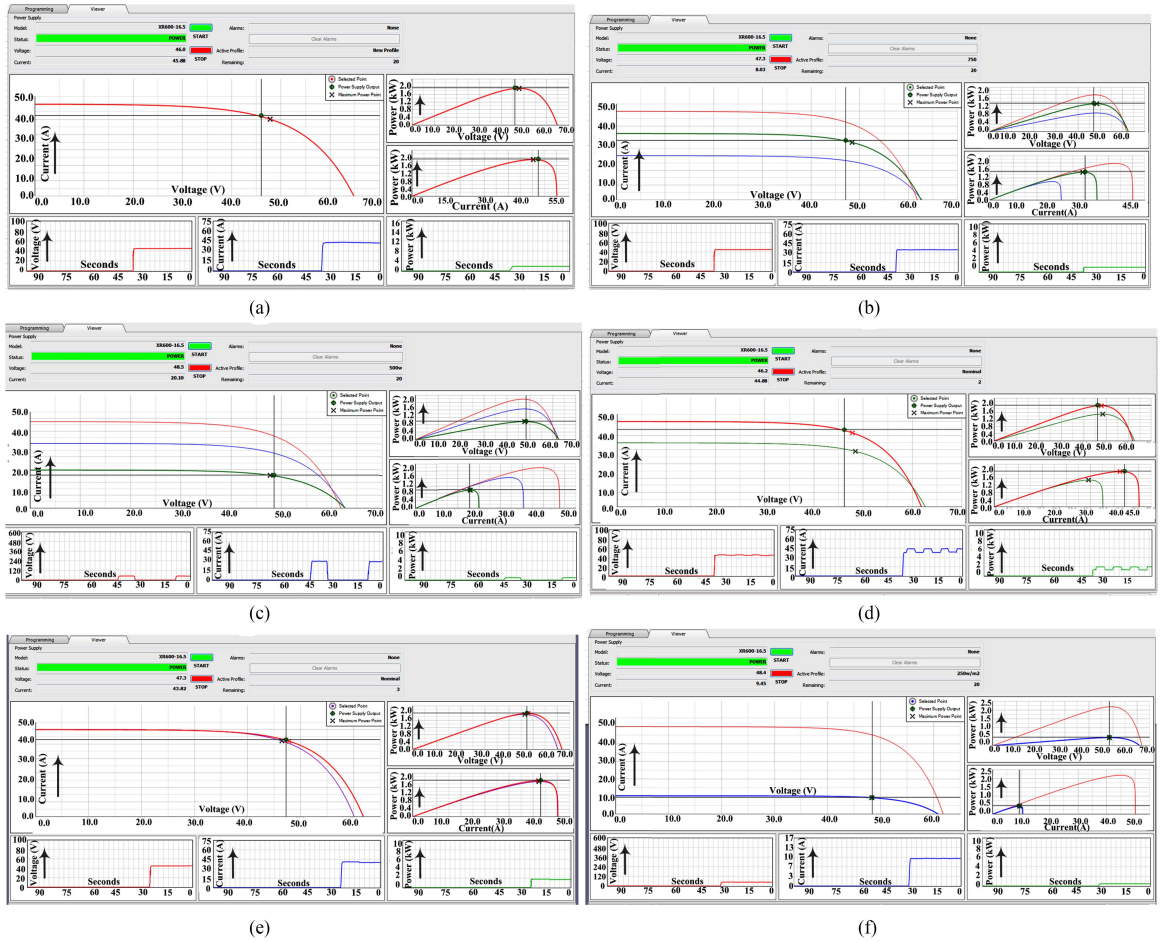

Fig. 6. Performance of proposed MPPT control, input voltage, current and power observed using solar PV characteristics from dc Programmable source, (a) at Irradiance 1000 W/m^2. (b) Irradiance 750 W/m^2. (c) Irradiance 500 W/m^2. (d) Irradiation changes from 1000 to 750 W/m^2. (e) Step change of Temperature from 25 °C to 40 °C. (f) Irradiation at 250 W/m^2.

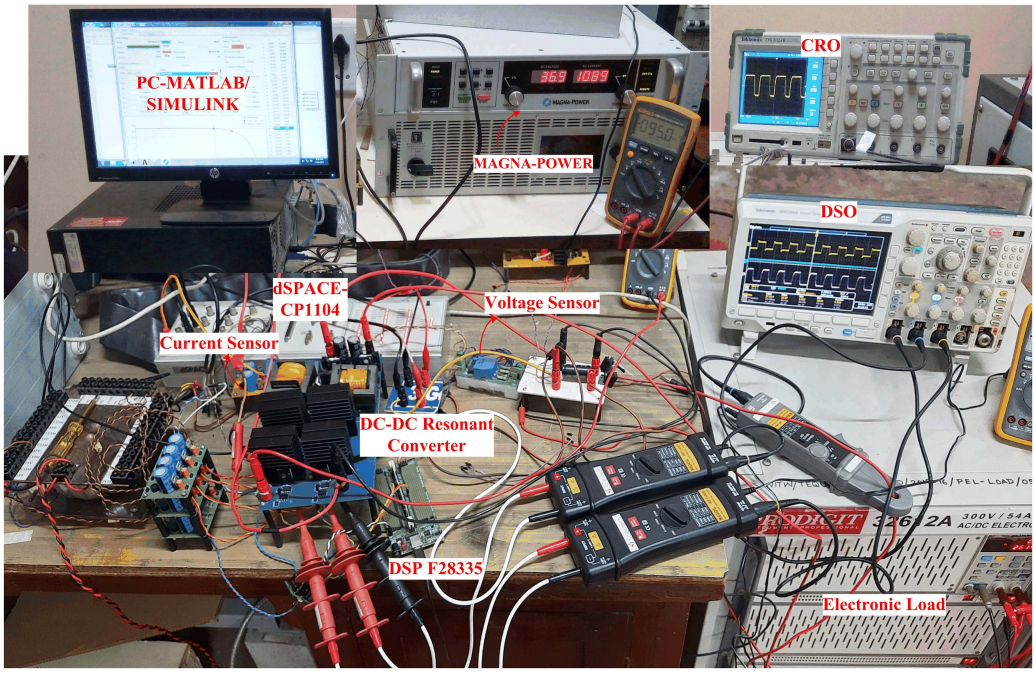

Fig. 7. Experimental setup of PV fed dc–dc converter.

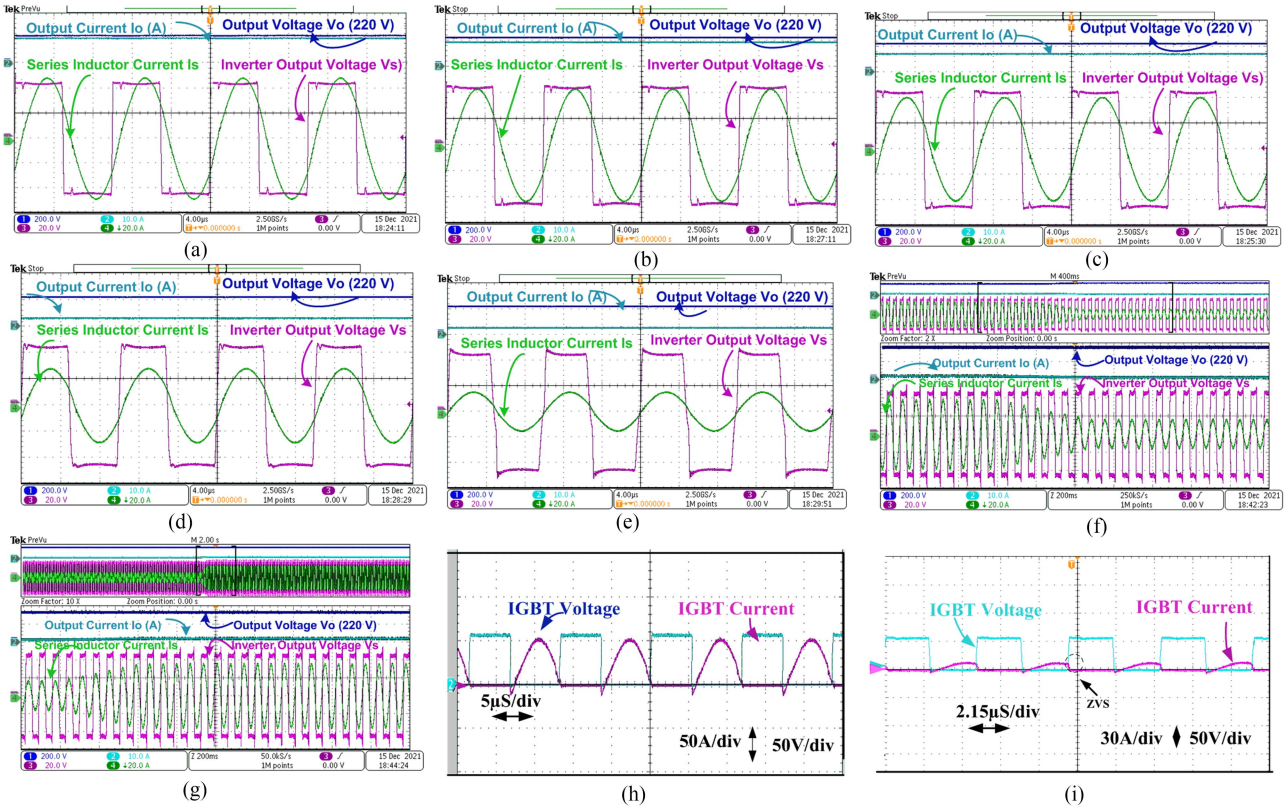

Fig. 8. Experimental results of the proposed resonant converter (HF inverter voltage, current and output voltage, current). (a) Output voltage regulation at 1000 W/m^2. (b) Regulation under Temperature change. (c) at 750 W/m^2 condition. (d) Irradiation 500 W/m^2 condition. (e) At 250 W/m^2. (f) Dynamic response for step change from 2200 to 1650 W. (g) From 1650 to 2200 W. (h) ZVS at full load. (i) ZVS at irradiation 250 W/m^2 condition.

on Magna-Power application, as shown in Fig. 6(d). The effect of temperature change from 25 °C to 40 °C is observed as shown in Fig. 6(e). As the temperature rises, the irradiance level falls, and the associated MPP falls. In Fig. 6(f) corresponds to an irradiation level of 250 W/m^2. Therefore, the developed dc–dc converter with proposed control technique effectively tracks the MPP of solar PV.

Fig. 8(a) shows for the solar PV power to the dc–dc converter at 1000 W/m^2, the proposed dual control method maintains the output voltage @220 V by adjusting D=0.48 and Y_s=104 kHz, respectively. At irradiation 750 W/m^2, the appropriate duty cycle (D)=0.43 and frequency Y_s=104 kHz were adjusted to maintain a constant output voltage, as shown in Fig. 8(b). From Fig. 8(c), the proposed dual control maintains the converter output voltage for 500 W/m^2 with duty cycle (D)=0.394 and frequency Y_s=107.3 kHz. Fig. 8(d) corresponds to irradiance level 250 W/m^2, the duty cycle $(D) = 0.36$ and Y_s=111.2 kHz, respectively, adjusted to regulate the required output voltage. In Fig. 8(e), as the temperature rises, the irradiation level falls, and the associated output power falls. Finally, the proposed dual control method is used to observe the performance converter for step changes in irradiance to verify the power converter's stability indirectly. Step change from 1000 to 750 W/m^2 and step change irradiance from 750 to 1000 W/m^2 are shown in Fig. 8(f) and (g). Table III summarizes the experimental results of the 2.2-kW prototype. The conversion efficiency of hard switched conventional converters is shown in Table IV. With

TABLE III
EXPERIMENTAL RESULTS OF PROPOSED 2.2-KW RESONANT CONVERTER

Variable	Full Load	75% Load	50% Load	25% Load
Irradiance W/m^2	1000	750	500	250
Power (W)	2200	1650	1100	550
Switching (Y_s) Frequency	104 kHz	104 kHz	107.3 kHz	111.2 kHz
Duty cycle (D)	0.48	0.43	0.397	0.36
R_L	22 Ω	29.33 Ω	44 Ω	88 Ω
Load current	10 A	7.5 A	5 A	2.5 A
Efficiency	97.3%	98.1%	98.7%	92%

TABLE IV
CONVERSION EFFICIENCY WITH CONVENTIONAL HARD SWITCHED CONVERTERS

S.	Energy conversion system component	Efficiency
1	DC–DC converter	Less than 90%
2	Boost converter	Less than 90%
3	Transformers, inductors, switching devices, gate driver circuits, digital signal processor, power supply	Less than 95%
4	Solar cell	Less than 25%
A	Overall system conversion efficiency (1 to 3) = 0.9 ×0.9 × 0.95	Less than 77%
B	Overall system conversion efficiency including solar cell (1 to 4) = 0.9× 0.9 × 0.95 × 0.25	**Less than 19.23%**

TABLE V
CONVERSION EFFICIENCY WITH SOFT-SWITCHED CONVERTERS

S.	Energy conversion system component	Efficiency
1	DC–DC Resonant converter	Greater than 98%
2	Transformers, inductors, switching devices,gate driver circuits,digital signal processor, power supply	Greater than 96%
3	Solar cell	Less than 44.5%
C	Overall system conversion efficiency (1 to 2) = 0.98 × 0.96	Greater than 94%
D	**Overall system conversion efficiency** including solar cell (1 to 3) = 0.98 × 0.96 × 0.445	**> 41.5%**
	% Rise in the overall system conversion efficiency (A to C)	**22.05%**
	% Rise in the overall system efficiency including solar cell (B to D)	**115.80%**

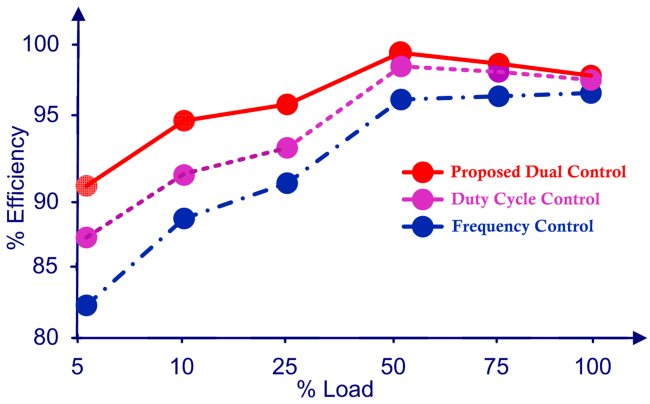

Fig. 9. Efficiency comparison with classical control technique

the proposed control method, we get a narrow range of operation of switching frequency even facilitating the ZVS of the power switches as shown in Fig. 8(h) and (i). Hence improves overall system power density and conversion efficiency, as indicated in Table V. To estimate the efficiency, output power, and input power are measured experimentally with proposed dual control and conventional control methods for the developed resonant converter over full load variation. Here, for the efficiency comparison shown in Fig. 9, the conventional frequency control, duty ratio control, and proposed dual control are implemented on the same developed hardware prototype for various loads. At 50% load, the developed converter has a maximum efficiency of 98.7%.

IV. CONCLUSION

Implementation of MPPT with dual controlled dc–dc resonant converter-based solar PV integration at various irradiance is presented. The power converter with duty cycle and duty cycle-frequency dual control is designed for effective PV utilization, output voltage regulation of the upstream resonant converter against PV voltage variations and sustained soft switching of the resonant converter over a comprehensive range with narrow frequency operation, and facilitates easy implementation in digital signal processors. A 2.2-kW prototype of the proposed converter-based solar PV integration is tested in the laboratory, and maximum efficiency is 98.7% attained at 50% load.

REFERENCES

[1] R. Gules, J. D. P. Pacheco, H. L. Hey, and J. Imhoff, "A maximum power point tracking system with parallel connection for PV stand-alone applications," *IEEE Trans. Ind. Electron*, vol. 55, no. 7, pp. 2674–2683, Jul. 2008.
[2] M. Liserre, T. Sauter, and J. Y. Hung, "Future energy systems: Integrating renewable energy sources into the smart power grid through industrial electronics," *IEEE Ind. Electron. Mag.*, vol. 4, no. 1, pp. 18–37, Mar. 2010.
[3] M. Meraj, S. Rahman, A. Iqbal, L. Ben-Brahim, and H. A. Abu -Rub, "Novel level-shifted PWM technique for equal power sharing among quasi-Z-source modules in cascaded multilevel inverter," *IEEE Trans. Power Electron.*, vol. 36, no. 4, pp. 4766–4777, Apr. 2021.
[4] O. Abdel-Rahim and H. Wang, "A new high gain DC-DC converter with model-predictive-control based MPPT technique for photovoltaic systems," *CPSS Trans. Power Electron.*, vol. 5, no. 2, pp. 191–200, Jun. 2020.
[5] M. Das and V. Agarwal, "Design and analysis of a high-efficiency DC–DC converter with soft switching capability for renewable energy applications requiring high voltage gain," *IEEE Trans. Ind. Electron*, vol. 63, no. 5, pp. 2936–2944, May 2016.
[6] S. Rahman, M. Meraj, A. Iqbal, L. Ben-Brahim, H. Abu -Rub, and I. Khan, "Novel level-shifted PWM technique for cascaded multilevel quasi-impedance source inverter," *IEEE J. Emerg. Sel. Topics Power Electron*, vol. 9, no. 5, pp. 5918–5928, Oct. 2021.
[7] A. K. Rathore, R. DevendraPatil, and D. Srinivasan, "Non-isolated bidirectional soft-switching current-fed LCL resonant DC/DC converter to interface energy storage in DC microgrid," *IEEE Trans. Ind. Appl*. vol. 52, no. 2, pp. 1711–1722, Mar./Apr. 2016.
[8] B. L. Narasimharaju, S. P. Dubey, and S. P. Singh, "Design and analysis of coupled inductor bidirectional DC-DC convertor for high voltage diversity," *IET Power Electron.*, vol. 5, no. 7, pp. 998–1007, 2012.
[9] H. Abu-Rub, A. Iqbal, and J. Guzinski, *High Performance Control of AC Drives with Matlab/Simulink*. Hoboken, NJ, USA: Wiley, 2021.
[10] T. Lodh, N. Pragallapati, and V. Agarwal, "Novel control scheme for an interleaved flyback converter based solar PV microinverter to achieve high efficiency," *IEEE Trans. Ind. Appl.*, vol. 54, no. 4, pp. 3473–3482, Jul./Aug. 2018.
[11] P. Nachankar, H. M. Suryawanshi, P. Chaturvedi, D. Atkar, and V. V. Reddy P., "Fault resilient soft switching DC–DC converter for modular solid state transformer applications," *IEEE Trans. Ind. Appl.*, vol. 58, no. 2, pp. 2242–2254, Mar. 2022.
[12] N. Shafiei, M. Pahlevaninezhad, H. Farzanehfard, and S. R. Motahari, "Analysis and implementation of a fixed-frequency LCLC resonant converter with capacitive output filter," *IEEE Trans. Ind. Electron*, vol. 58, no. 10, pp. 4773–4782, Oct. 2011.
[13] H. M. Suryawanshi and S. G. Tarnekar, "Resonant converter in high power factor, high voltage DC application," *IEE Proc-Elect. Power Appl.*, vol. 145, no. 4, pp. 307–314, Jul. 1998.
[14] R. Lin and L. Huang, " Efficiency improvement on LLC resonant converter using integrated LCLC resonant transformer," *IEEE Trans. Ind. Appl*, vol. 54, no. 2, pp. 1756–1764, Mar. 2018.
[15] E. Asa, K. Colak, and D. Czarkowski, "Analysis of a CLL resonant converter with semi-bridgeless active rectifier and hybrid control," *IEEE Trans. Ind. Electron.*, vol. 62, no. 11, pp. 6877–6886, Nov. 2015.
[16] H. Park and J. Jung, "PWM and PFM hybrid control method for LLC resonant converters in high switching frequency operation," *IEEE Trans. Ind. Electron.*, vol. 64, no. 1, pp. 253–263, Jan. 2017.
[17] D. Panda and V. Ramanarayanan, "Modelling and simulation of switched reluctance motor drive," *J. Indian Inst. Sci.*, vol. 80, no. 4, Aug. 2000, Art. no. 333.
[18] Y. Chen et al., "LCLC converter with optimal capacitor utilization for hold-up mode operation," *IEEE Trans. Power Electron.*, vol. 34, no. 3, pp. 2385–2396, Mar. 2019.
[19] S. Ryu et al., "Adjustable frequency– duty-cycle hybrid control strategy for full-bridge series resonant converters in EV chargers," *IEEE Trans. Ind. Electron.*, vol. 61, no. 10, pp. 5354–5362, Oct. 2014.

Vijaya Vardhan Reddy P received the B.Tech. degree in electrical and electronics engineering from PBR VITS, Kavali, India, in 2009, the M.Tech. degree in control system engineering from the Indian Institute of Technology Kharagpur, Kharagpur, India, in 2013, and the Ph.D. degree in electrical engineering with the Visvesvaraya National Institute of Technology, Nagpur, India, in 2020.

During 2014, he was an IP Professional with GE Global Research, Bangalore, India. He is currently a Lead Product Engineer with Varroc Engineering LTD, Aurangabad, India. His research interests include dc–dc converter, soft-switched resonant converter, and control system.

B L Narasimharaju (Senior Member, IEEE) received B.E. and M.E. degrees from the University Visvesvaraya College of Engineering (UVCE), Bangalore, India, in 1999 and 2002, respectively, and the Ph.D. from the Indian Institute of Technology Roorkee (IIT Roorkee), Roorkee, India, in 2012, all in electrical engineering.

He was a Project Trainee with ABB Bangalore and LRDE, Ministry of Defence, Bengaluru, India. He was a Teaching Assistant with UVCE, from April 2002 to August 2003. Since August 2003 to May 2012, he was a Faculty of Electrical Engineering, MIT, Manipal University, Manipal, India. He is currently a Professor of Electrical Engineering, National Institute of Technology, Warangal, India. His research areas power conversion, control techniques, electric drives, and applications.

Hiralal Murlidhar Suryawanshi (Fellow, IEEE) received the B.E. degree from the Walchand College of Engineering, Sangli, India, in 1988, the M.E. degree from the Indian Institute of Science, Bangalore, India, in 1994, and the Ph.D. degree from Nagpur University, Nagpur, India, in 1999, all in electrical engineering.

He is currently the Director of the National Institute of Technology, Hamirpur, India. He is also a Professor (HAG) with the Department of Electrical Engineering, Visvesvaraya National Institute of Technology, Nagpur, India. His research interests include the field of power electronics, emphasizing developmental work of resonant converters, power factor correction, active power filters, FACTs devices, multilevel converters, electric drives, etc.

Dr. Suryawanshi became a Fellow of the Indian National Academy of Engineering (INAE), India, in 2012 for his outstanding research. He is conferred with the Abdul Kalam Technology Innovation National Fellowship by the INAE and Department of Science and Technology, Government of India. He is also a Chair Professor of the INAE. He is currently an Associate Editor of IEEE TRANSACTION ON INDUSTRIAL ELECTRONICS and IEEE OPEN JOURNAL OF THE INDUSTRIAL ELECTRONICS SOCIETY.